~~RESTRICTED~~

RM No. L8F16

NACA RM No. L8F16

27 SEP 1949 UNCLASSIFIED

NACA

RESEARCH MEMORANDUM

LOW-SPEED PRESSURE DISTRIBUTIONS OVER THE DROOPED-NOSE FLAP OF A 42° SWEPTBACK WING WITH CIRCULAR-ARC AIRFOIL SECTIONS AT A REYNOLDS NUMBER OF 5.3×10^6

By

Stanley H. Spooner and Robert L. Woods

Langley Aeronautical Laboratory
Langley Field, Va.

NATIONAL ADVISORY COMMITTEE FOR AERONAUTICS

WASHINGTON

September 23, 1948

NACA RM No. L8F16

NATIONAL ADVISORY COMMITTEE FOR AERONAUTICS

RESEARCH MEMORANDUM

LOW-SPEED PRESSURE DISTRIBUTIONS OVER THE DROOPED-NOSE FLAP OF A 42° SWEPTBACK WING WITH CIRCULAR-ARC AIRFOIL SECTIONS AT A REYNOLDS NUMBER OF 5.3×10^6

By Stanley H. Spooner and Robert L. Woods

SUMMARY

The pressure distributions over the drooped-nose flap of a 42° sweptback wing having circular-arc airfoil sections and equipped with half-span trailing-edge split flaps have been investigated in the Langley 19-foot pressure tunnel. The wing had an aspect ratio of 3.94 and a taper ratio of 0.625. The pressure measurements were made for several angles of attack at a Reynolds number of 5.3×10^6 and a Mach number of 0.11. The effects of the deflection and span of the drooped-nose flap and the effects of split trailing-edge flaps on the pressures over the drooped-nose flap were determined.

The maximum values of pressure coefficient were measured at the inboard end of the drooped-nose flap; whereas, on the remaining portion of the flap where considerable cross flow existed, large pressure peaks were not measured. At angles of attack near maximum lift the center of load on the flap shifted markedly inboard.

The normal-force and hinge-moment coefficients of the nose flap increased almost linearly with angle of attack and decreased linearly with increased nose-flap deflection for angles of attack below those at which flow separation occurred. The angle of attack at which separation occurred increased with increased nose deflection. Maximum values of the drooped-nose-flap normal-force and hinge-moment coefficients of 2.1 and 1.2, respectively, were obtained. The effect of variation in the drooped-nose-flap span on the maximum values of the coefficients was small, whereas removal of the split flaps reduced the maximum values about 0.2.

INTRODUCTION

The use of wings incorporating thin, circular-arc airfoil sections in supersonic aircraft design has resulted in a need for high-lift

and stall-control devices in order to provide acceptable take-off and landing characteristics. One of several proposed devices consists of a rotatable or drooped leading edge. Although there is a limited amount of two-dimensional data available concerning the aerodynamic forces and moments acting on the drooped-nose flap of sharp-edge airfoil sections (reference 1), little is known about the three-dimensional characteristics of such a device when used on a sweptback wing. Pressure-distribution measurements have, therefore, been made over the drooped leading edge of a 42° sweptback wing having circular-arc airfoil sections. The basic characteristics of this wing are given in reference 2.

The effects of variation in deflection and span of the drooped leading edge together with the effects of trailing-edge split flaps were determined. The investigation was conducted in the Langley 19-foot pressure tunnel at a Reynolds number of approximately 5.3×10^6 and a Mach number of 0.11.

SYMBOLS

C_L lift coefficient (Lift/qS)

P pressure coefficient $\left(\frac{p - p_o}{q}\right)$

P_R resultant pressure coefficient

C_{N_f} drooped-nose-flap normal-force coefficient $\left(\int_0^1 c_{n_f} \frac{c_f}{c_f'} d\left(\frac{y_f}{b_f}\right)\right)$

C_{h_f} drooped-nose-flap hinge-moment coefficient $\left(\int_0^1 c_{h_f} \frac{c_f^2}{\bar{c}_f^2} d\left(\frac{y_f}{b_f}\right)\right)$

c_{n_f} drooped-nose-flap section normal-force coefficient, positive upward $\left(\int_0^1 P_R \, d\left(\frac{x_f}{c_f}\right)\right)$

c_{h_f} drooped-nose-flap section hinge-moment coefficient, positive when leading edge tends to deflect upward $\left(\int_0^1 P_R \frac{x_f}{c_f} d\left(\frac{x_f}{c_f}\right)\right)$

q free-stream dynamic pressure

S wing area

p orifice pressure

p_o free-stream static pressure

$b/2$ semispan of wing, normal to plane of symmetry

c_f local chord of drooped-nose flap, normal to hinge line

c_f' mean chord of drooped-nose flap, normal to hinge line

$\bar{c}_f$ root-mean-square chord of drooped-nose flap, normal to hinge line

b_f span of drooped-nose flap, measured along hinge line

y_f spanwise coordinate, measured from inboard end of drooped-nose flap along hinge line

x_f chordwise coordinate, measured from and normal to hinge line

c.p. chordwise center of pressure of drooped-nose flap, measured from leading edge normal to hinge line

α angle of attack of wing chord, degrees

δ_f deflection of drooped-nose flap, degrees

MODEL AND TESTS

The principal dimensions of the model are shown in figure 1. The wing was of solid steel construction and is described in detail in reference 2. It had an aspect ratio of 3.94 and a ratio of tip chord to root chord of 0.625. A straight line connecting the leading edge of the root and theoretical tip chords was swept back 42.05°. The airfoil sections were symmetrical circular arcs which, taken normal to the line of maximum thickness, had a maximum thickness of 10 percent of the chord at the root and 6.4 percent of the chord at the tip. Parallel to the plane of symmetry the maximum thickness was 7.9 percent of the chord at the root and 5.2 percent of the chord at the tip.

The drooped nose was hinged on the lower surface and had a chord of approximately 18.4 percent of the wing chord measured parallel to the plane of symmetry. Two drooped-nose-flap spans were tested: one covering the outboard 60 percent of the wing semispan and the other, the outboard 75 percent. The drooped-nose flap was so constructed as to provide deflections of 0°, 20°, 30°, and 40°.

The trailing-edge split flaps were 20 percent of the wing chord and were deflected 60°. They covered the inboard 50 percent of the wing semispan.

Flush static pressure orifices were installed in the drooped nose at five spanwise stations as shown in figure 2. Chordwise, there were normally nine upper-surface and three lower-surface orifices, the locations of which may be determined from the pressure-distribution diagrams. The tubing connecting the orifices in the model to the measuring apparatus was installed in a manner such that it interfered with neither the distribution nor the measurement of the forces. The pressures over the drooped-nose flap were measured on a multiple-tube manometer and were photographically recorded for several angles of attack. In addition to the pressure measurements, force measurements of the lift were made for the various model configurations. For the majority of the tests the wing was equipped with the split flaps. The data have been corrected for airstream misalinement, model blocking, support tare, and jet-boundary effects.

The tests were conducted in the Langley 19-foot pressure tunnel at a Reynolds number of approximately 5.3×10^6 and a Mach number of about 0.11.

RESULTS AND DISCUSSION

The lift curves for the various configurations tested are presented in figure 3. Representative chordwise pressure distributions are presented in figures 4 to 6. For the undeflected-nose-flap configuration (fig. 4(a)) separated flow over the nose section is indicated by the flat tops of the pressure-distribution diagrams throughout the angle-of-attack range. With the nose flap deflected the maximum negative values of pressure coefficient occurred at the inboard ends of both the short- and long-span drooped noses. The pressure coefficients increased with angle of attack and decreased with increased nose deflection. Higher values were obtained for the long-span nose-flap configurations than for the short-span nose-flap configurations. A wing of plan form similar to that used in the present tests but with NACA 64-series airfoil section and a round-nose, extensible leading-edge flap gave somewhat higher maximum values of pressure coefficient (reference 3).

The stall studies presented in figure 7 appear to correlate well with the pressure-distribution diagrams of figure 4(c). For moderate and high angles of attack, considerable cross flow on the drooped-nose flap was evident, except at the inboard end where the flow was straight back. The highest negative pressure peaks were measured at the inboard end of the drooped-nose flap, whereas over the areas with cross flow large negative pressure peaks were not obtained. These peaks at the inboard end were somewhat higher than those obtained in two-dimensional tests (reference 1) even though lower peaks would be expected for the sweptback wing. At the high angles of attack areas of separated flow on the drooped-nose flap occurred on the outboard portion of the flap and moved inboard with increasing angle of attack. This is shown by the stall studies and verified by the pressure-distribution diagrams.

The chordwise center of pressure at various angles of attack is shown in figure 4(c) for the short-span drooped-nose flap. The center of

pressure at each of the spanwise stations moved forward with angle of attack until at moderate to high angles it remained approximately constant at about 45 percent of the nose-flap chord behind the leading edge. Neither the removal of the split flaps nor the change to the longer span nose flap had any appreciable effect on the center-of-pressure locations. Although the centers of pressure are presented only for one configuration, they are representative of the other configurations.

The section normal-force and hinge-moment coefficients are presented in table I for all of the configurations investigated. The chord-force coefficients are not presented but were determined for several cases and found to average about 5 percent of the corresponding normal-force coefficients. The spanwise loading on the drooped-nose flap is given in figures 8 to 10 for several configurations. In general, it can be seen that from low to moderate angles of attack the center of load was shifted outboard slightly; whereas, at angles of attack near those for maximum lift, stalling on the outer portion of the nose-flap span caused the center of load to be shifted markedly to the inboard portion. The removal of the half-span trailing-edge split flaps caused the center of load to be shifted somewhat outboard.

The spanwise loadings were mechanically integrated to determine the drooped-nose-flap normal-force and hinge-moment coefficients which are presented in figures 11 to 13. The force and moment coefficients for the nose-flap-deflected conditions increased almost linearly with angle of attack up to angles at which separation occurred. For the undeflected condition $\left(\delta_f = 0^\circ\right)$ C_N and C_h remained approximately constant due to separation which began at low angles of attack. The values of C_N and C_h, at a given angle of attack below that at which separation occurred, decreased proportionally with increase in nose-flap deflection for the range investigated. The angle of attack at which separation occurred was increased with increased nose-flap deflection.

Although the drooped-nose-flap normal-force and hinge-moment coefficients increased more rapidly with angle of attack for the long-span drooped-nose flap $\left(0.75\frac{b}{2}\right)$ than for the short-span flap $\left(0.60\frac{b}{2}\right)$, the maximum forces and moments of the long-span flap were reached at a lower angle of attack and were approximately equal to those of the short-span flap. These values were about 2.1 and 1.2, respectively, for the normal-force and hinge-moment coefficients. The maximum normal-force coefficients of the drooped-nose flap were only about 60 percent as large as those obtained on the extensible leading-edge flap of reference 3.

The effect of the half-span trailing-edge split flaps may be seen in figure 13. At a given angle of attack removal of the split flaps reduced the drooped-nose-flap normal-force and hinge-moment coefficients by increments of approximately 0.4 and 0.3, respectively, for the range of linear variation with angle of attack. At the higher angles of attack

the values of C_N and C_h for the configuration $0.60\frac{b}{2}$-span drooped-nose flap and $\delta_f = 30^\circ$ were reduced about 0.2 by removal of the split flaps.

CONCLUDING REMARKS

The results of an investigation of the pressure distribution over the drooped-nose flap of a sweptback wing incorporating circular-arc airfoil sections and equipped with half-span trailing-edge split flaps indicate that large negative pressure peaks are not obtained where cross flow on the flap is evident. The maximum value of pressure coefficient was obtained at the inboard end of the drooped-nose flap where no cross flow was present. At angles of attack in the vicinity of the maximum lift the loading on the drooped-nose flap shifted markedly toward the inboard end.

The drooped-nose-flap normal-force and hinge-moment coefficients increased almost linearly with angle of attack and decreased proportionally with increase in nose deflection for angles of attack below those at which flow separation occurred. The angle of attack at which separation occurred was increased with increased nose-flap deflection. The maximum values of drooped-nose-flap normal-force and hinge-moment coefficients obtained were approximately 2.1 and 1.2, respectively, and were not appreciably affected by the nose-flap span.

Removal of the split flaps reduced the drooped-nose-flap normal-force and hinge-moment coefficients by 0.4 and 0.3, respectively, for the range of linear variation with angle of attack. At higher angles of attack, however, the values were reduced about 0.2.

Langley Aeronautical Laboratory
National Advisory Committee for Aeronautics
Langley Field, Va.

REFERENCES

1. Underwood, William J., and Nuber, Robert J.: Aerodynamic Load Measurements over Leading-Edge and Trailing-Edge Plain Flaps on a 6-Percent-Thick Symmetrical Circular-Arc Airfoil Section. NACA RM No. L7H04, 1947.

2. Neely, Robert H., and Koven, William: Low-Speed Characteristics in Pitch of a 42° Sweptback Wing with Aspect Ratio 3.9 and Circular-Arc Airfoil Sections. NACA RM No. L7E23, 1947.

3. Conner, D. William, and Foster, Gerald V.: Investigation of Pressure Distribution over an Extended Leading-Edge Flap on a 42° Sweptback Wing. NACA RM No. L7J03, 1947.

Table I.- Section Normal-Force and Hinge-Moment Coefficients.

0.60b/2-span drooped nose; half-span split flaps										
	$\frac{y_f}{b_f}$ / α	c_{h_f}				c_{n_f}				C_L
		0.05	0.33	0.60	0.88	0.05	0.33	0.60	0.88	
$\delta_f = 0°$	4.8	0.92	0.65	0.51	0.37	1.77	1.20	0.93	0.68	0.72
	8.9	.84	.56	.48	.39	1.64	1.04	.90	.74	.86
	13.0	.71	.56	.43	.36	1.36	1.03	.82	.70	.91
	17.0	.71	.55	.50	.41	1.41	1.05	.96	.77	.93
	19.0	.72	.59	.52	.43	1.43	1.12	.98	.80	.95
	21.0	.72	.61	.51	.42	1.47	1.17	1.00	.79	.96
$\delta_f = 20°$	4.8	0.47	0.42	0.30	0.20	0.96	0.88	0.76	0.55	0.67
	9.0	.71	.87	.20	.61	1.28	1.61	1.56	1.17	.87
	13.1	1.03	1.77	.95	.60	1.73	2.30	1.93	1.21	1.07
	15.2	1.25	1.42	.84	.58	2.05	2.86	1.61	1.07	1.12
	17.2	1.33	1.29	.78	.55	2.25	2.76	1.56	1.08	1.17
	19.3	1.11	1.91	.89	.56	1.89	2.63	1.80	1.13	1.23
$\delta_f = 30°$	4.7	0.22	0.20	0.14	0.04	0.67	0.60	0.55	0.21	0.65
	8.9	.48	.59	.56	.35	1.02	1.22	1.16	.60	.83
	13.1	.76	.97	1.03	.74	1.37	1.78	1.82	1.25	.99
	17.2	1.01	1.28	1.28	.86	1.71	2.42	2.44	1.48	1.13
	19.3	1.07	1.38	1.13	.80	1.80	2.79	2.19	1.40	1.19
	21.3	1.20	1.55	1.02	.77	2.02	3.03	2.00	1.35	1.24
$\delta_f = 40°$	4.7	0.07	0.06	-0.10	-0.08	0.46	0.32	0.13	-0.09	0.64
	8.9	.27	.30	.27	.22	.73	.92	.85	.39	.85
	13.1	.49	.63	.68	.46	.99	1.37	1.43	.78	.99
	17.2	.68	.94	1.01	.74	1.22	1.82	1.90	1.16	1.10
	19.2	.81	1.10	1.17	.83	1.42	2.11	2.17	1.29	1.16
	21.3	.82	1.21	1.25	.83	1.46	2.40	2.32	1.31	1.21

Table I.- Continued.

0.75b/2-span drooped nose; half-span split flaps													
	$\frac{y_f}{b_f}$ / α	c_{h_f}					c_{n_f}					C_L
		0.04	0.24	0.46	0.68	0.90	0.04	0.24	0.46	0.68	0.90	
$\delta_f = 0°$	4.8	0.95	0.92	0.65	0.51	0.37	1.74	1.77	1.20	0.93	0.68	0.72
	8.9	1.14	.84	.56	.48	.39	2.31	1.64	1.04	.90	.74	.86
	13.0	.88	.71	.56	.43	.36	1.75	1.36	1.03	.82	.70	.91
	17.0	.80	.71	.55	.50	.41	1.56	1.41	1.05	.96	.77	.93
	19.0	.71	.72	.59	.52	.43	1.53	1.43	1.12	.98	.80	.95
	21.0	.80	.72	.61	.51	.42	1.57	1.47	1.17	1.00	.79	.96
$\delta_f = 20°$	4.7	0.32	0.48	0.41	0.31	0.20	0.78	0.99	0.87	0.74	0.58	0.65
	8.9	.68	1.02	.93	.88	.64	1.28	1.82	1.70	1.61	1.20	.84
	13.1	1.07	1.43	1.00	.73	.57	1.85	2.78	2.00	1.46	1.10	1.05
	15.2	1.31	1.56	.99	.70	.54	2.22	3.15	1.94	1.38	1.06	1.12
	17.2	1.42	1.42	.91	.65	.51	2.39	2.93	1.79	1.30	1.00	1.17
	18.2	.82	1.19	.82	.63	.51	2.47	2.42	1.63	1.17	.98	1.18
$\delta_f = 30°$	4.8	0.15	0.24	0.18	0.16	0.02	0.54	0.75	0.61	0.55	0.11	0.66
	8.9	.45	.68	.63	.58	.38	1.00	1.41	1.30	1.22	.51	.86
	13.1	.81	1.16	1.12	1.07	.77	1.83	2.11	2.10	2.01	1.31	1.04
	16.3	1.03	1.54	1.22	.97	.70	1.89	2.70	2.43	1.95	1.26	1.17
	18.4	1.24	1.70	1.13	.88	.56	2.13	3.13	2.27	1.77	1.01	1.23
	20.4	1.38	1.42	.94	.66	.47	2.38	2.88	1.91	1.32	.85	1.24
$\delta_f = 40°$	4.7	0.09	0.10	0.07	-0.11	-0.08	0.20	0.39	0.29	0.11	-0.07	0.63
	8.9	.22	.37	.32	.28	.20	.71	.97	.98	.88	.36	.85
	13.1	.98	.79	.79	.72	.46	1.12	1.59	1.68	1.57	.72	1.01
	17.2	.82	1.24	1.20	1.13	.73	1.62	2.23	2.33	2.19	1.12	1.16
	19.3	.95	1.46	1.30	1.13	.75	1.81	2.66	2.55	2.18	1.16	1.24
	21.3	1.24	1.58	1.11	.96	.63	2.15	2.96	2.23	1.87	1.00	1.26

Table I.- Concluded.

0.60b/2-span drooped nose										
	$\frac{y_f}{b_f}$ / α	c_{h_f}				c_{n_f}				c_L
		0.55	0.33	0.60	0.88	0.05	0.33	0.60	0.88	
δ_f = 30°	4.3	-0.14	-0.13	-0.14	-0.08	0.09	0.06	-0.11	-0.03	0.22
	8.5	.18	.19	.18	.14	.54	.61	.59	.49	.44
	12.7	.41	.52	.57	.45	.82	1.08	1.15	.95	.64
	16.9	.65	.92	1.01	.79	1.18	1.70	1.80	1.52	.82
	20.0	.83	1.18	1.05	.73	1.49	2.31	2.06	1.44	.99
	21.1	.97	1.17	.94	.66	1.73	2.42	1.88	1.33	1.06
	23.2	1.21	1.15	.92	.55	2.10	2.32	1.73	1.09	1.13
	24.2	1.24	1.25	.84	.55	2.15	2.56	1.68	1.12	1.13

NACA

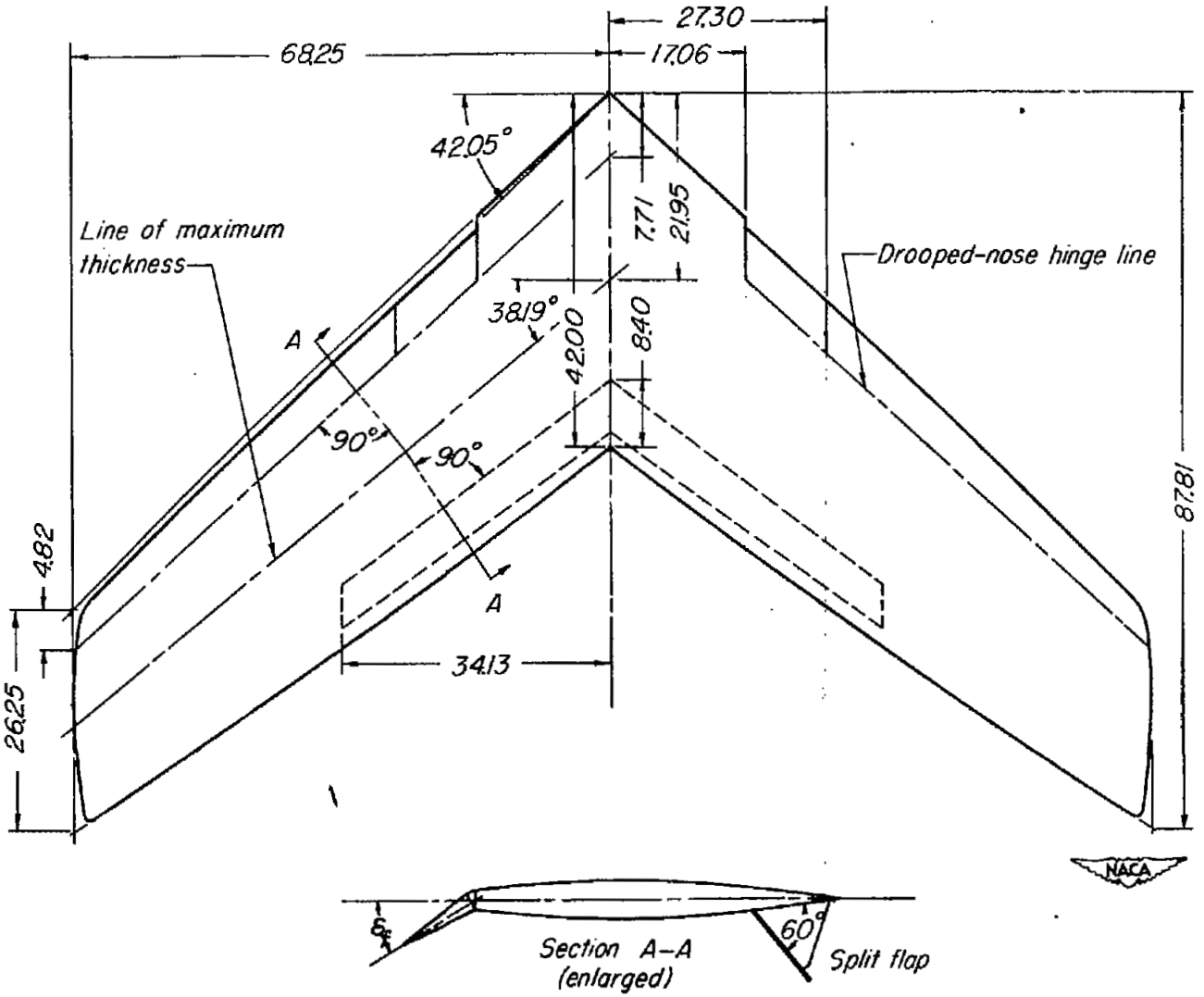

Figure 1.- Geometry of wing. All dimensions in inches.

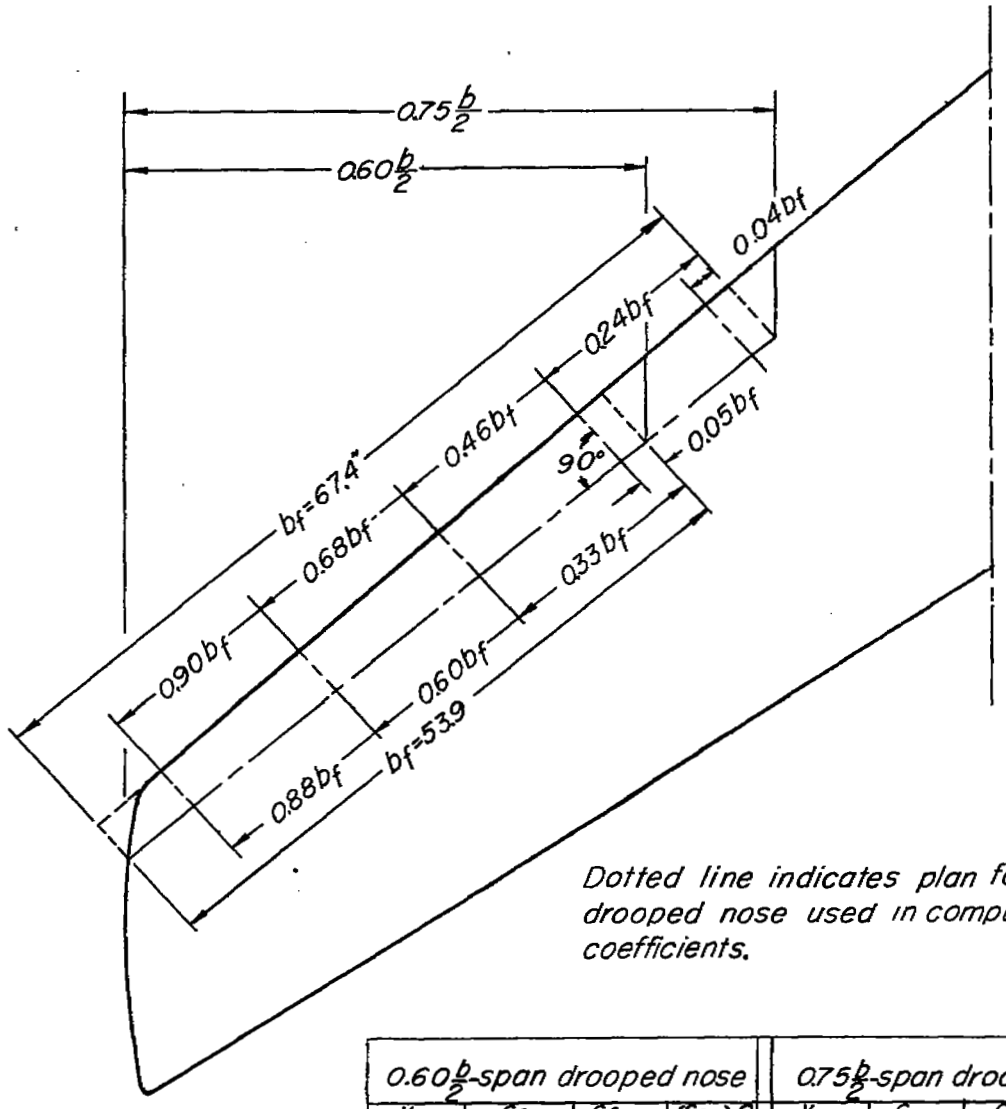

Dotted line indicates plan form of drooped nose used in computation of coefficients.

$0.60\frac{b}{2}$-span drooped nose				$0.75\frac{b}{2}$-span drooped nose			
y_f/b_f	c_f	c_f/c'_f	$(c_f/c'_f)^2$	y_f/b_f	c_f	c_f/c'_f	$(c_f/c'_f)^2$
0.05	5.09	1.15	1.32	0.04	5.38	1.17	1.35
.33	4.72	1.06	1.15	.24	5.09	1.10	1.21
.60	4.25	.96	.92	.46	4.72	1.02	1.04
.88	3.72	.84	.71	.68	4.25	.92	.85
				.90	3.72	.81	.64

NACA

Figure 2.- Spanwise location of pressure orifices.

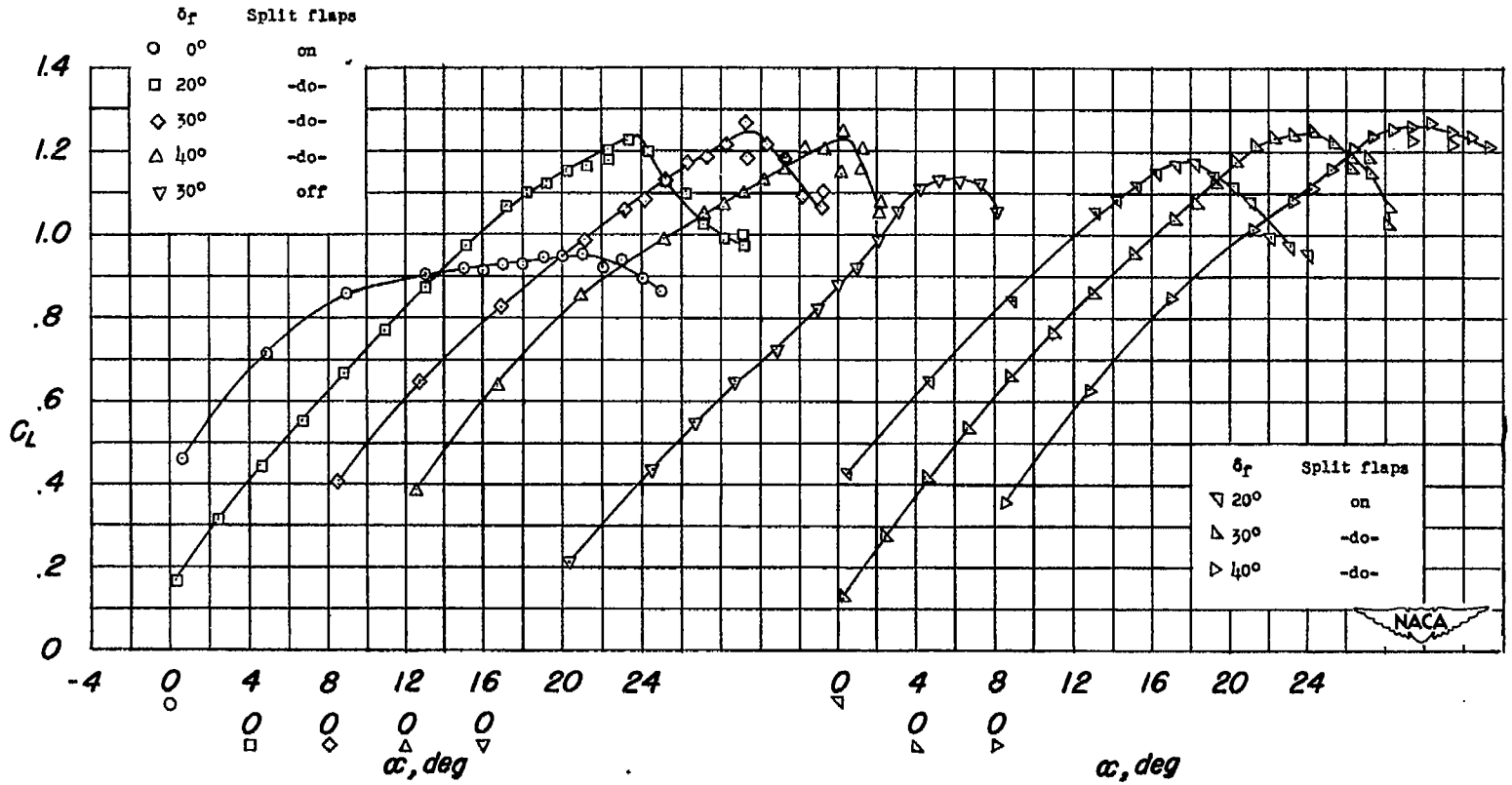

(a) $0.60\frac{b}{2}$-span drooped nose.

(b) $0.75\frac{b}{2}$-span drooped nose.

Figure 3.- Lift characteristics of 42° sweptback wing.

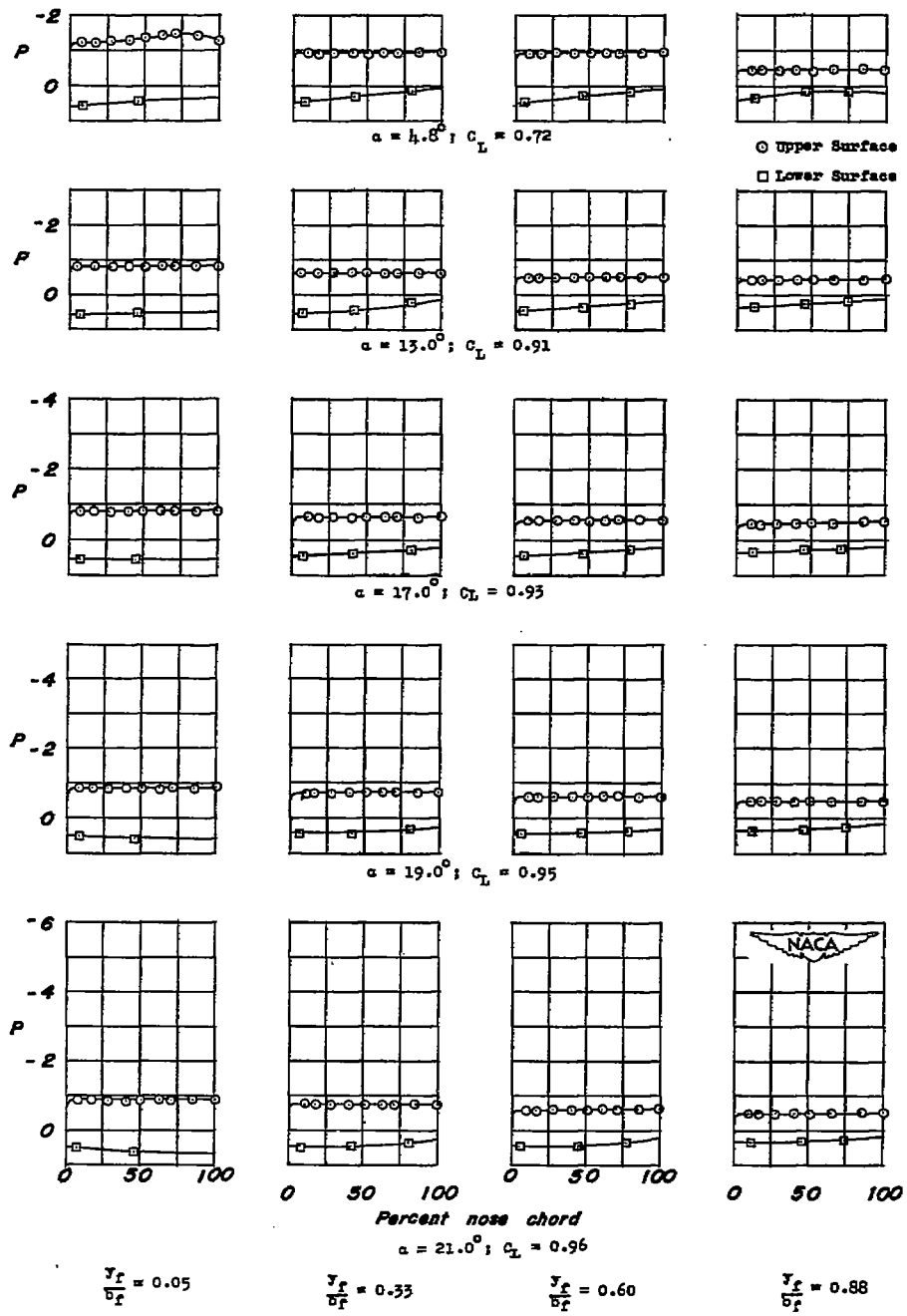

(a) $\delta_f = 0^\circ$.

Figure 4.- Pressure distribution over $0.60\frac{b}{2}$-span drooped nose. Half-span split flaps deflected 60°.

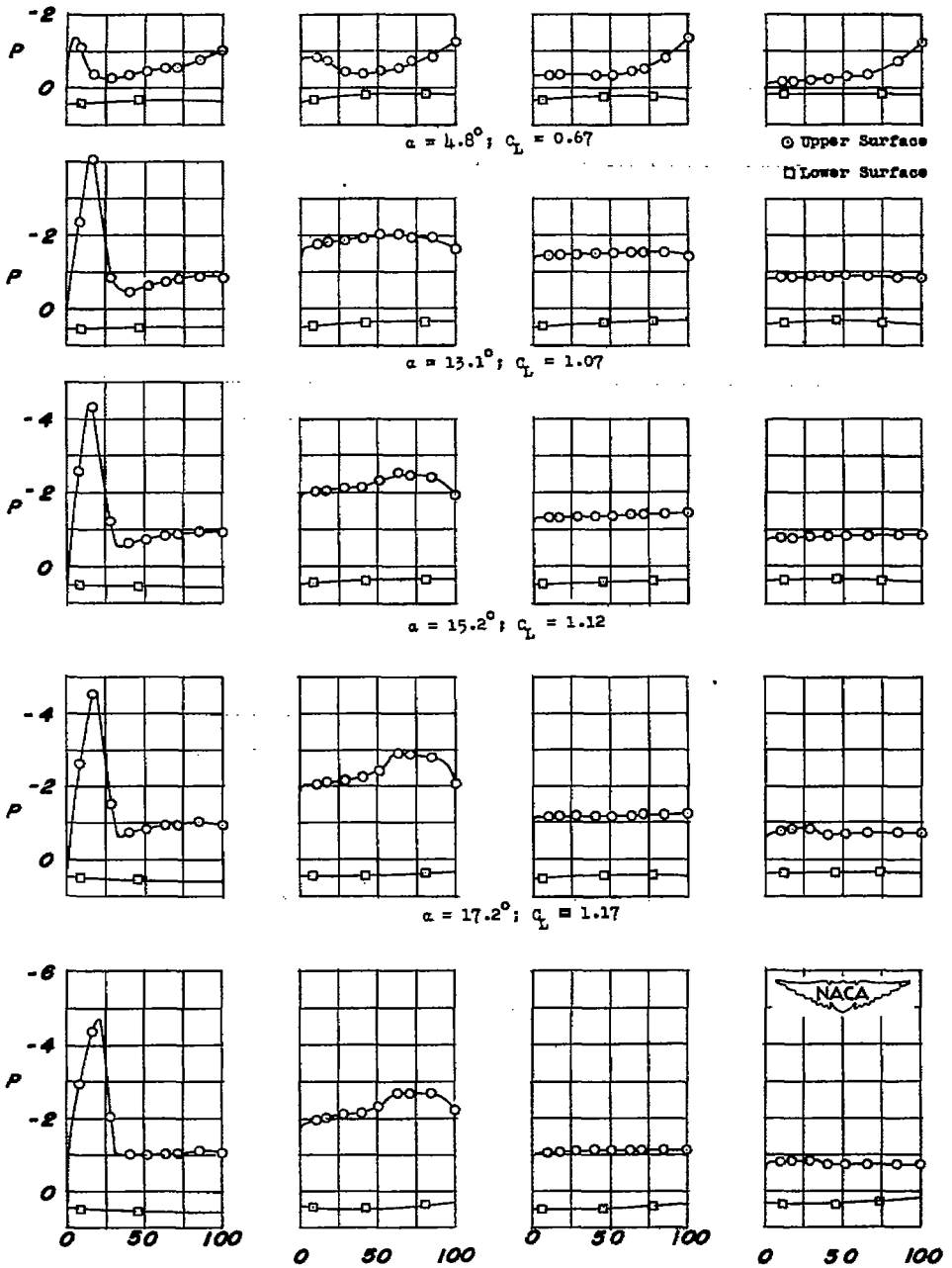

(b) $\delta_f = 20^\circ$.

Figure 4.- Continued.

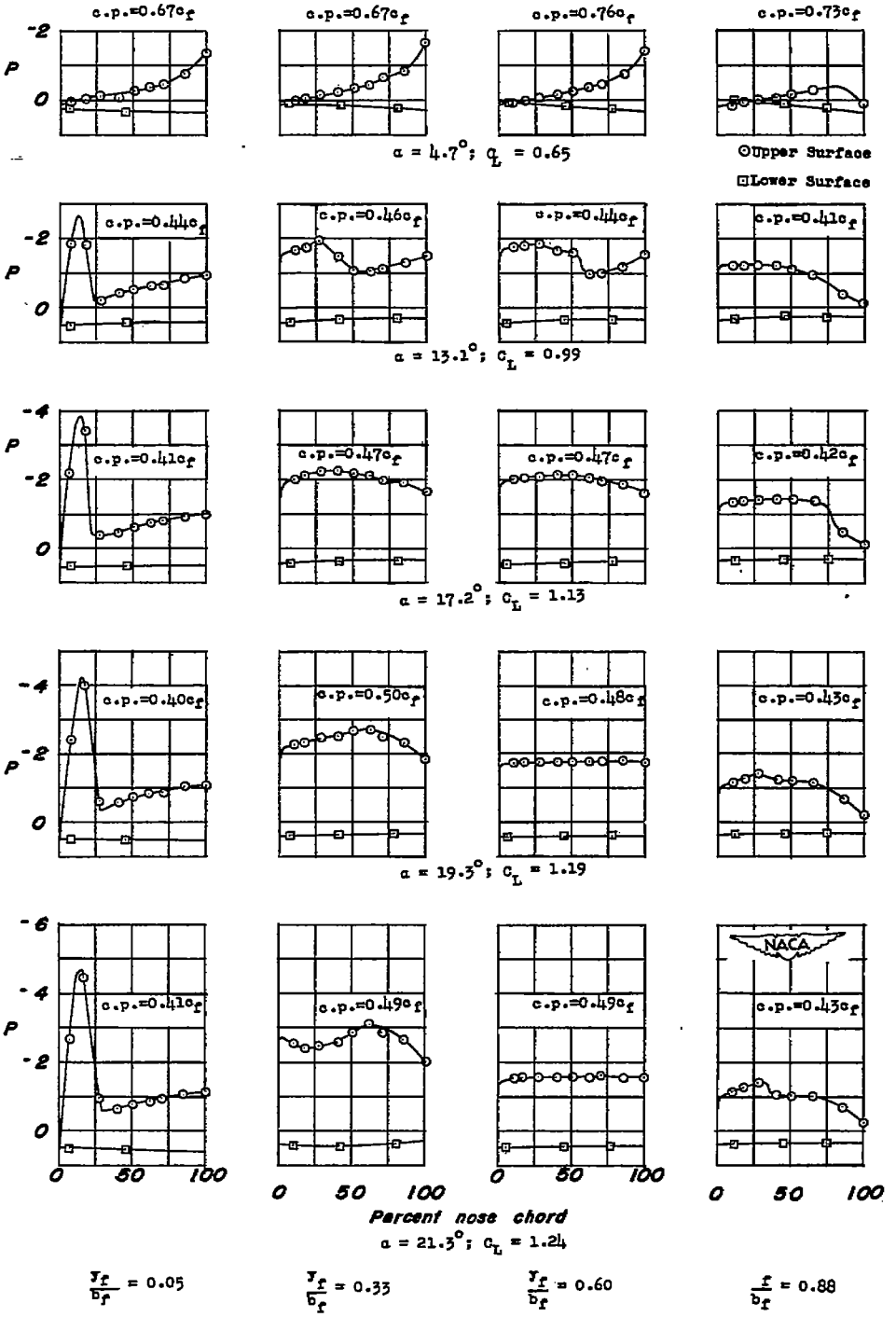

(c) $\delta_f = 30°$.

Figure 4.- Continued.

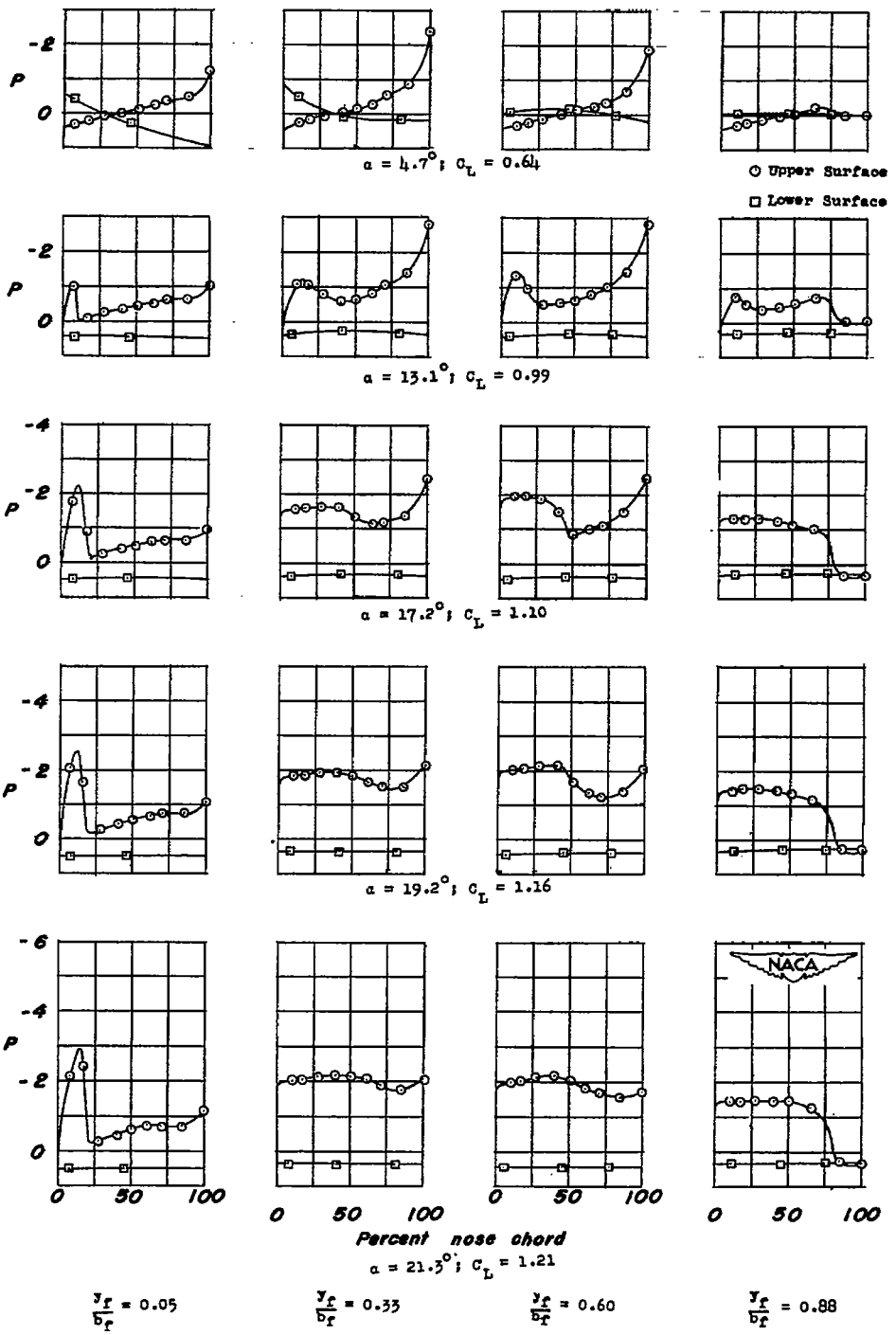

(d) $\delta_f = 40^\circ$.

Figure 4.- Concluded.

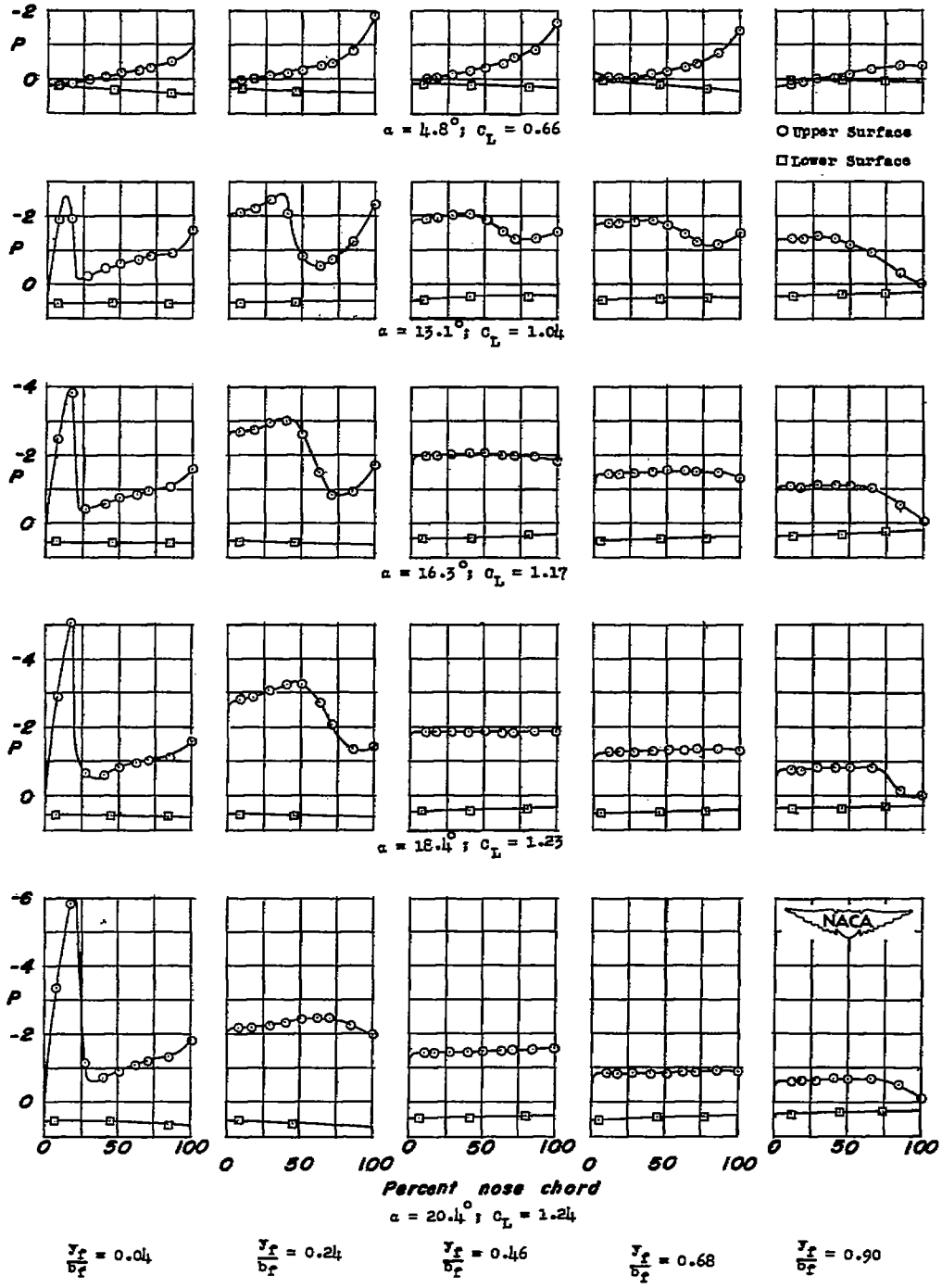

Figure 5.- Pressure distribution over $0.75\frac{b}{2}$-span drooped nose. $\delta_f = 30^\circ$; half-span split flaps deflected 60°.

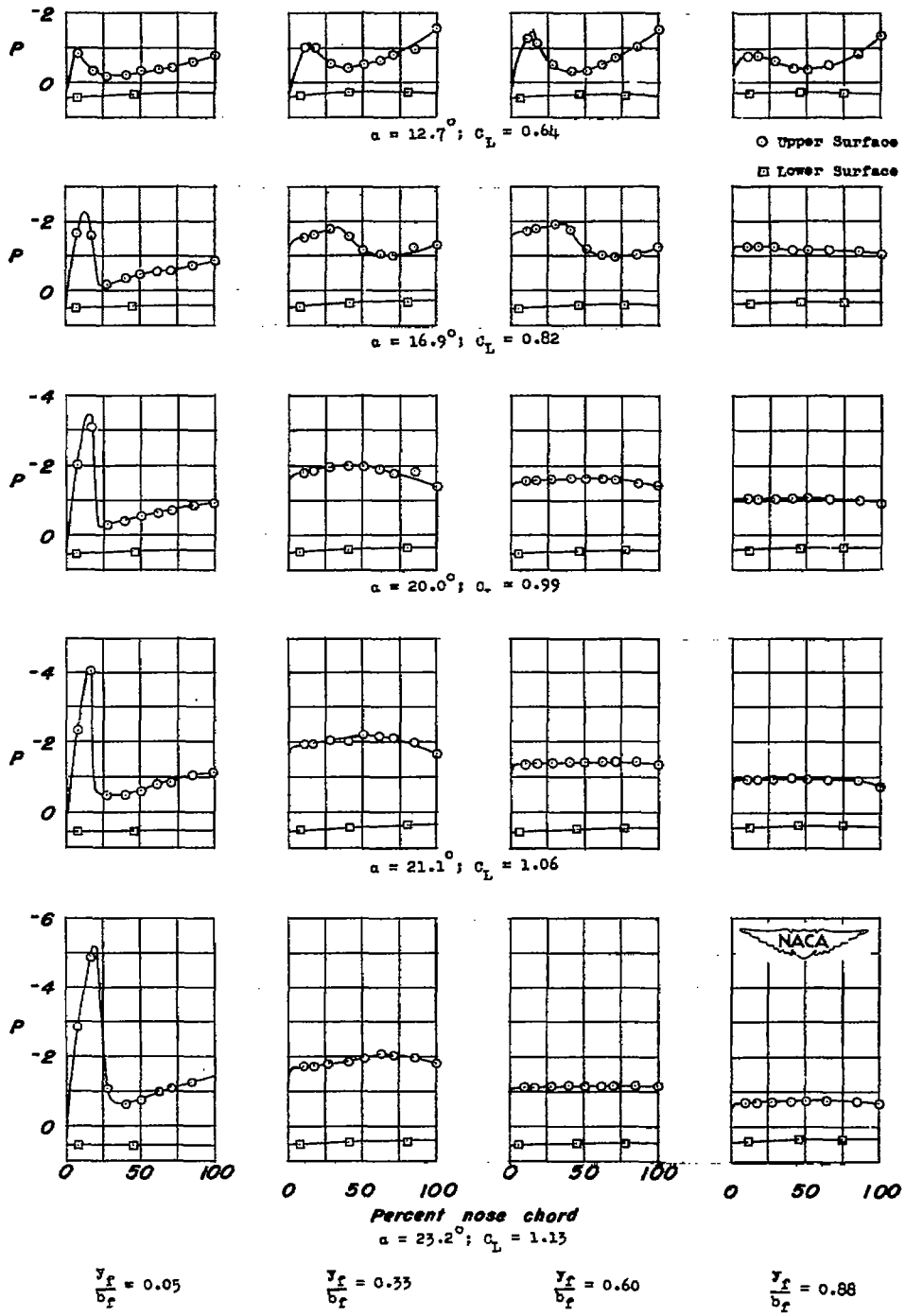

Figure 6.- Pressure distribution over $0.60\frac{b}{2}$-span drooped nose. $\delta_f = 30^\circ$; split flaps off.

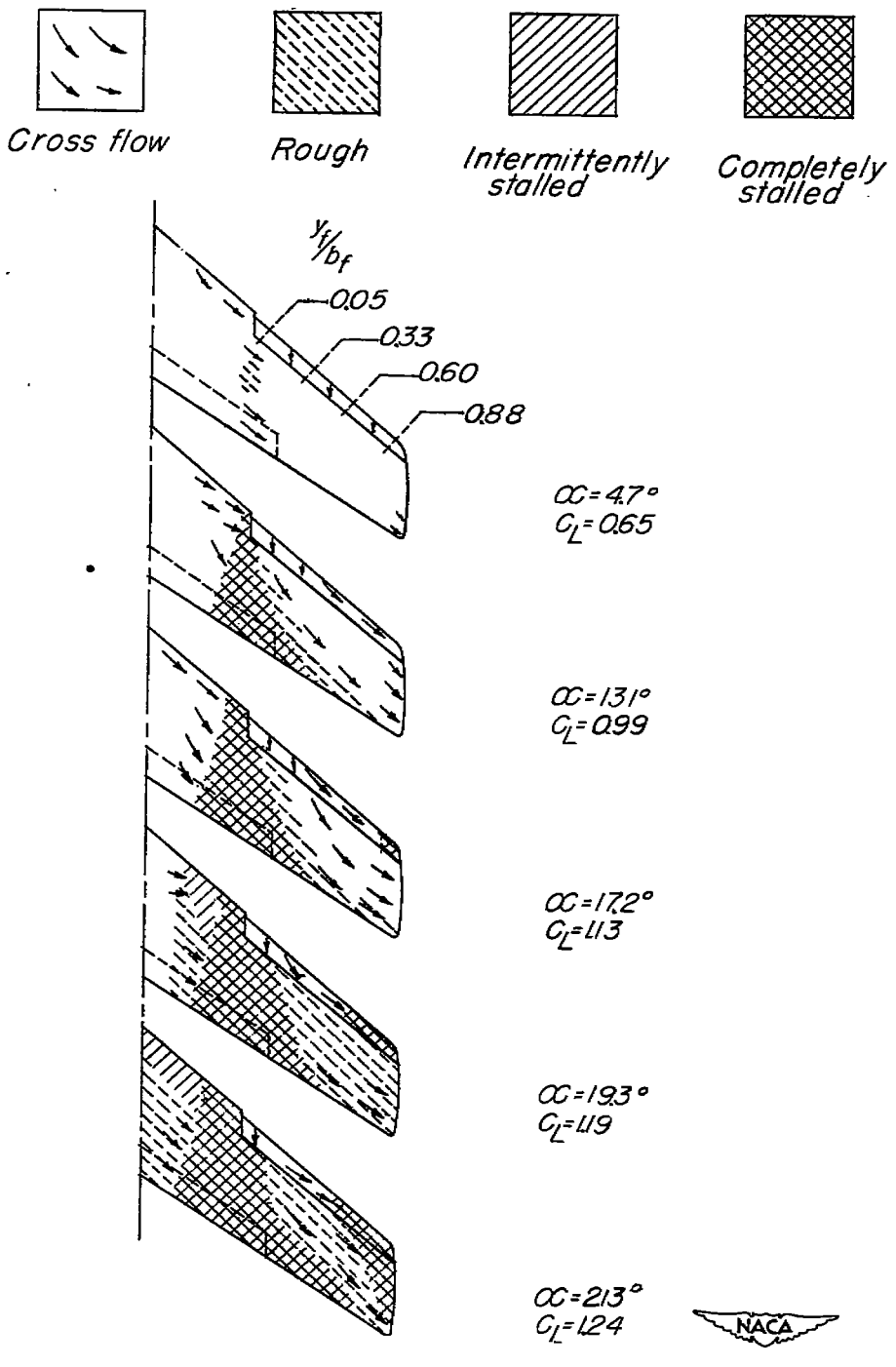

Figure 7.- Stalling characteristics of wing. $\delta_f = 30°$; $b_f = 0.60\frac{b}{2}$; $0.50\frac{b}{2}$ split flaps deflected 60°.

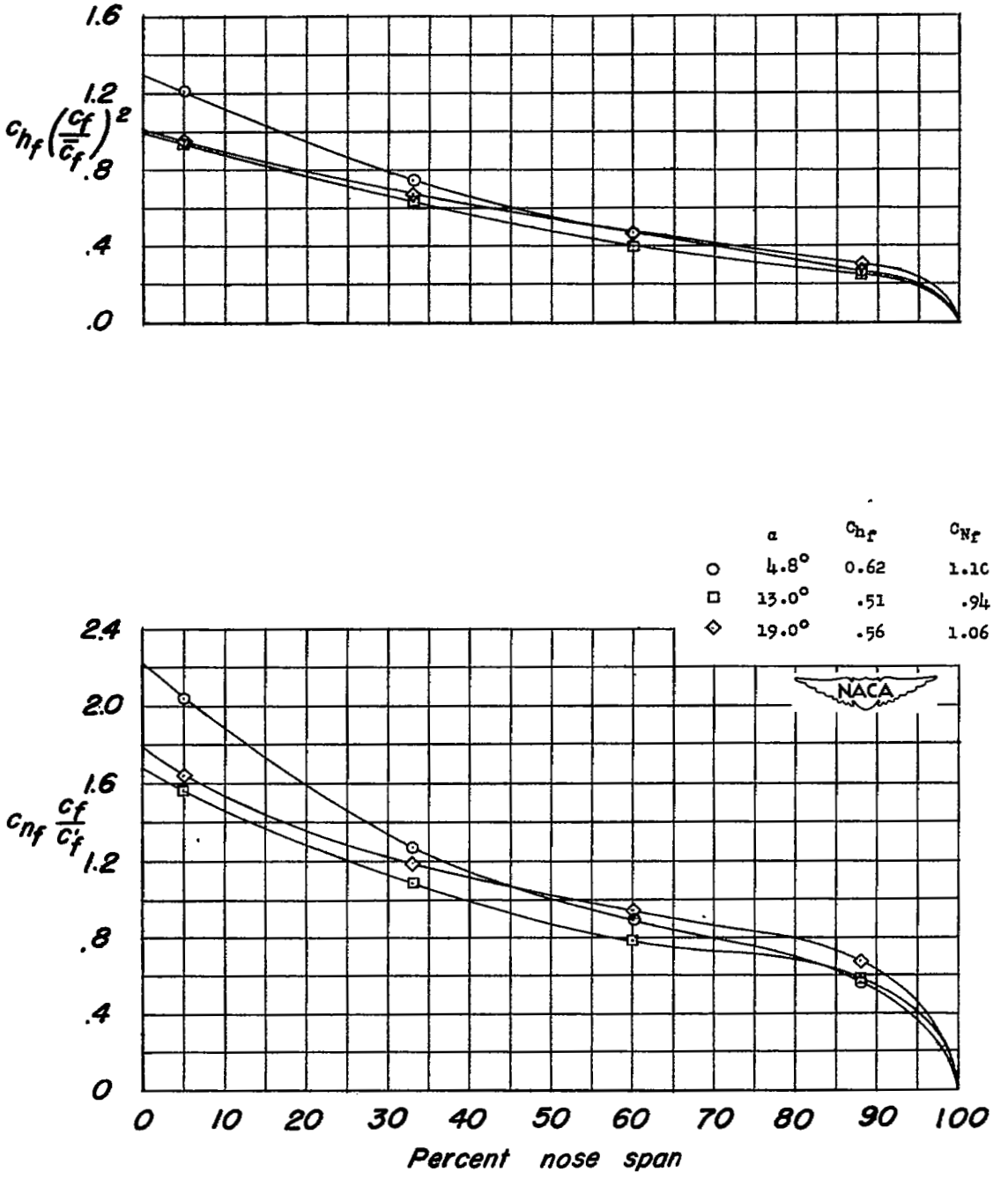

(a) $\delta_f = 0^\circ$.

Figure 8.- Spanwise variation of drooped-nose normal-force and hinge-moment coefficients. $0.60\frac{b}{2}$ span drooped nose; half-span split flaps deflected 60°.

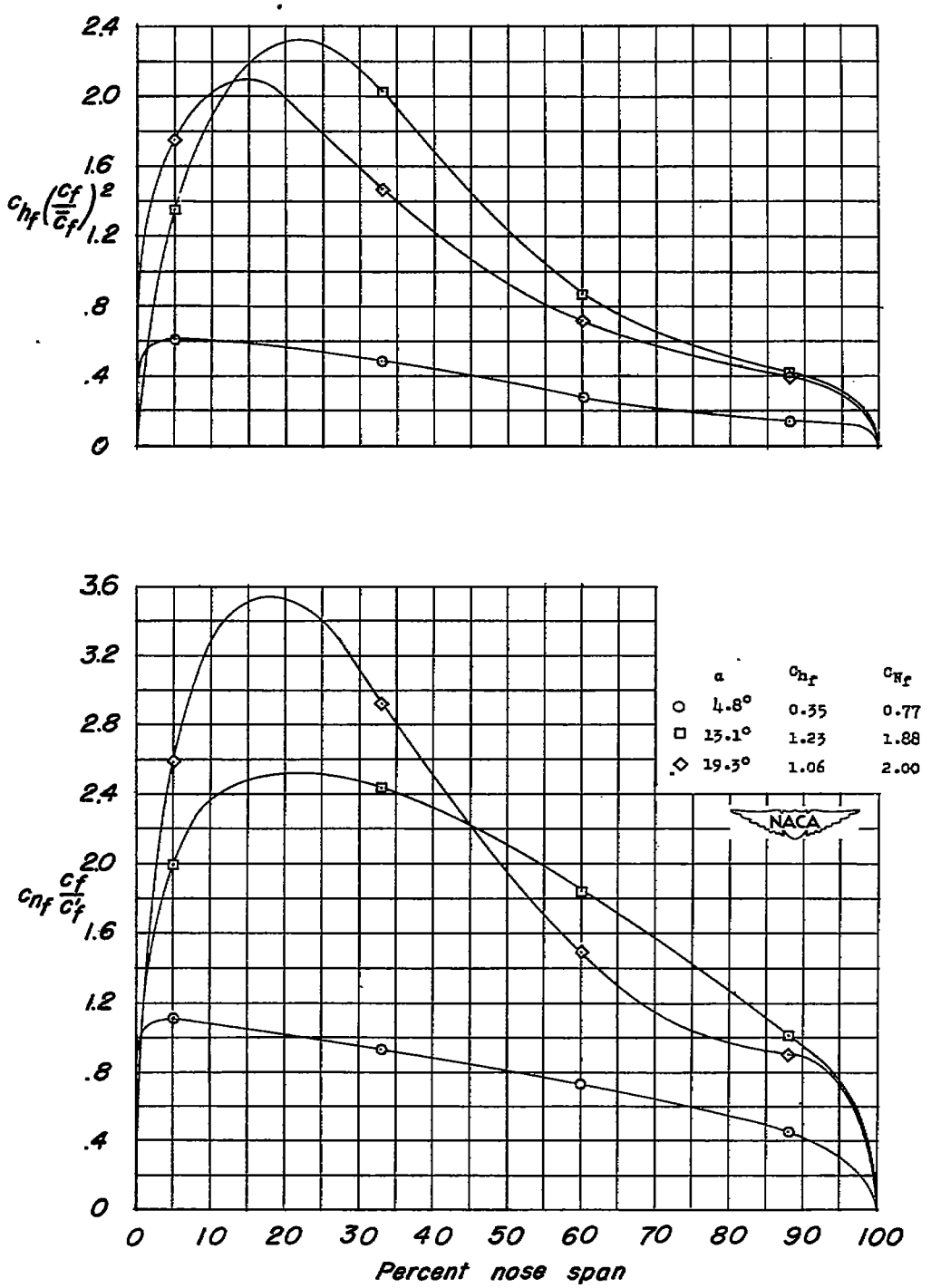

(b) $\delta_f = 20^\circ$.

Figure 8.- Continued.

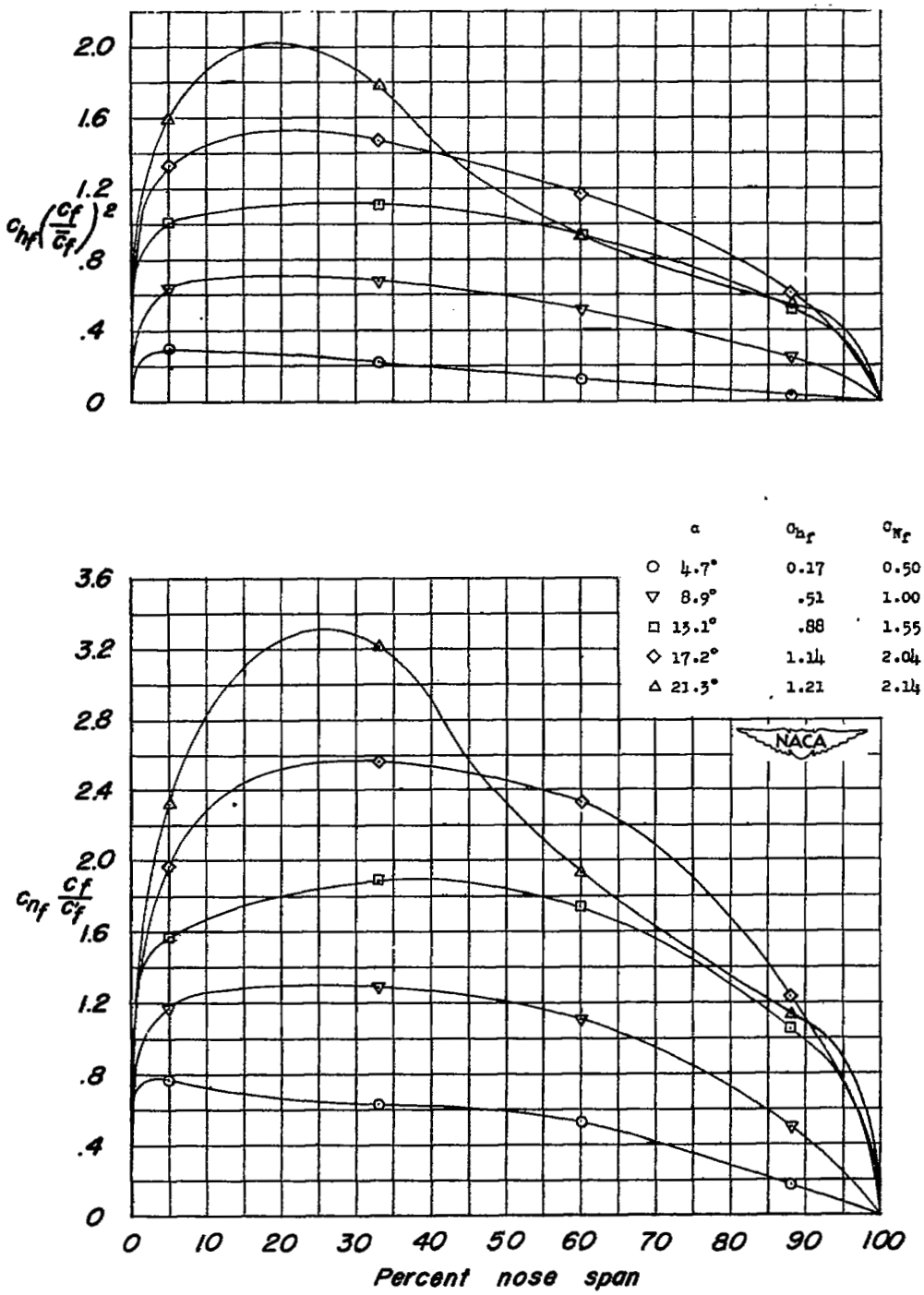

(c) $\delta_f = 30^\circ$.

Figure 8.- Continued.

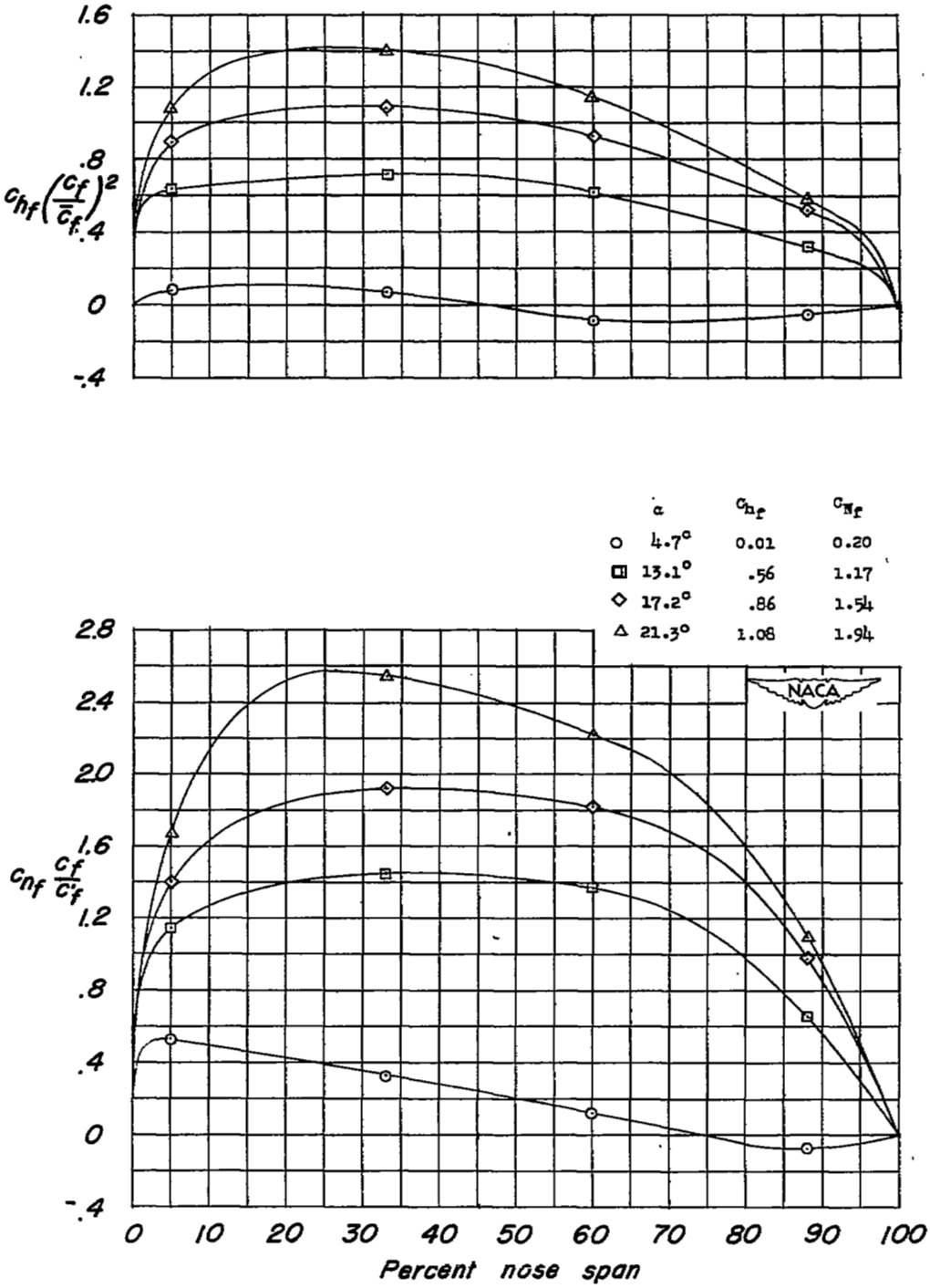

(d) $\delta_f = 40^\circ$.

Figure 8.- Concluded.

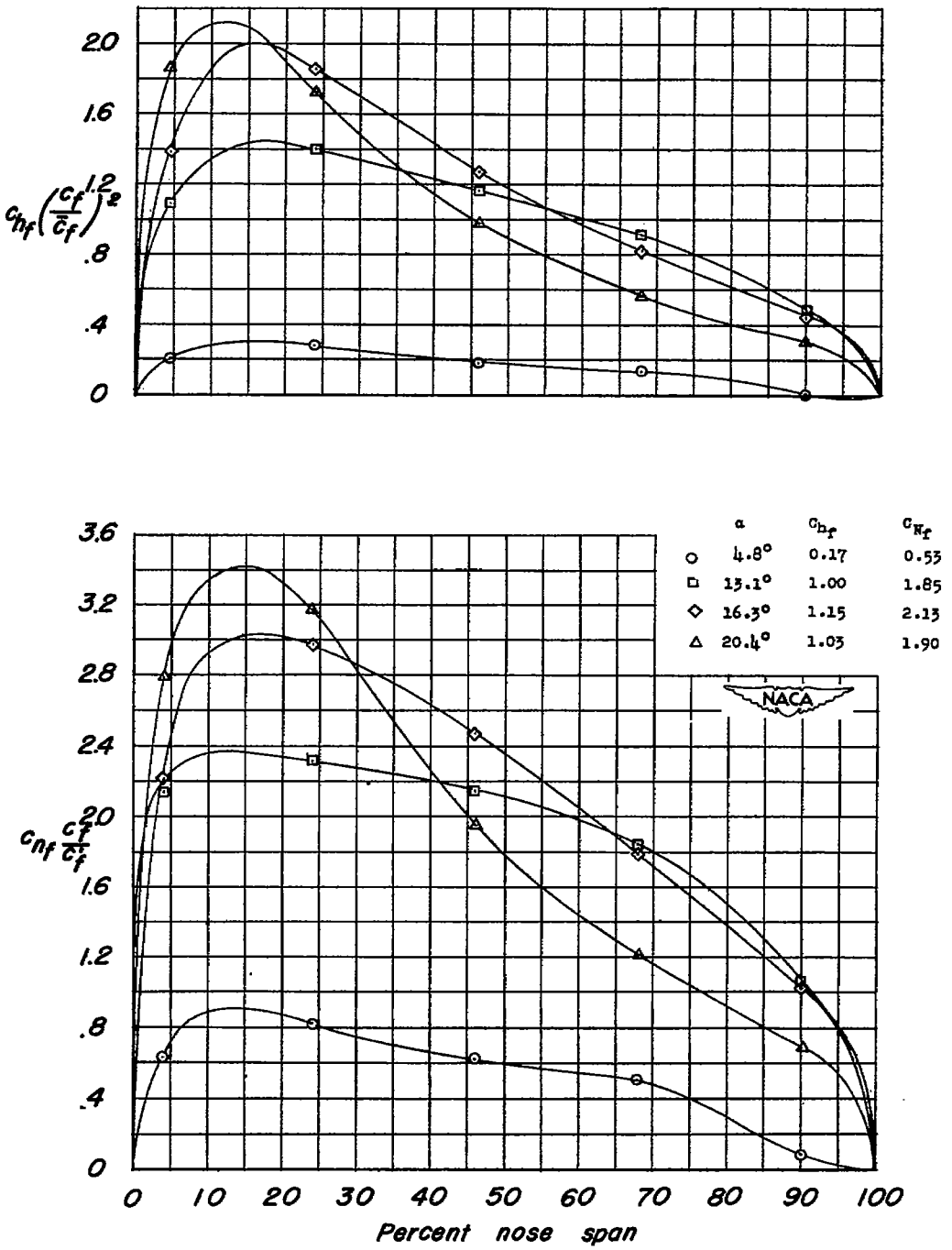

Figure 9.- Spanwise variation of drooped-nose normal-force and hinge-moment coefficients. $0.75\frac{b}{2}$-span drooped nose; $\delta_f = 30^\circ$; half-span split flaps deflected 60°.

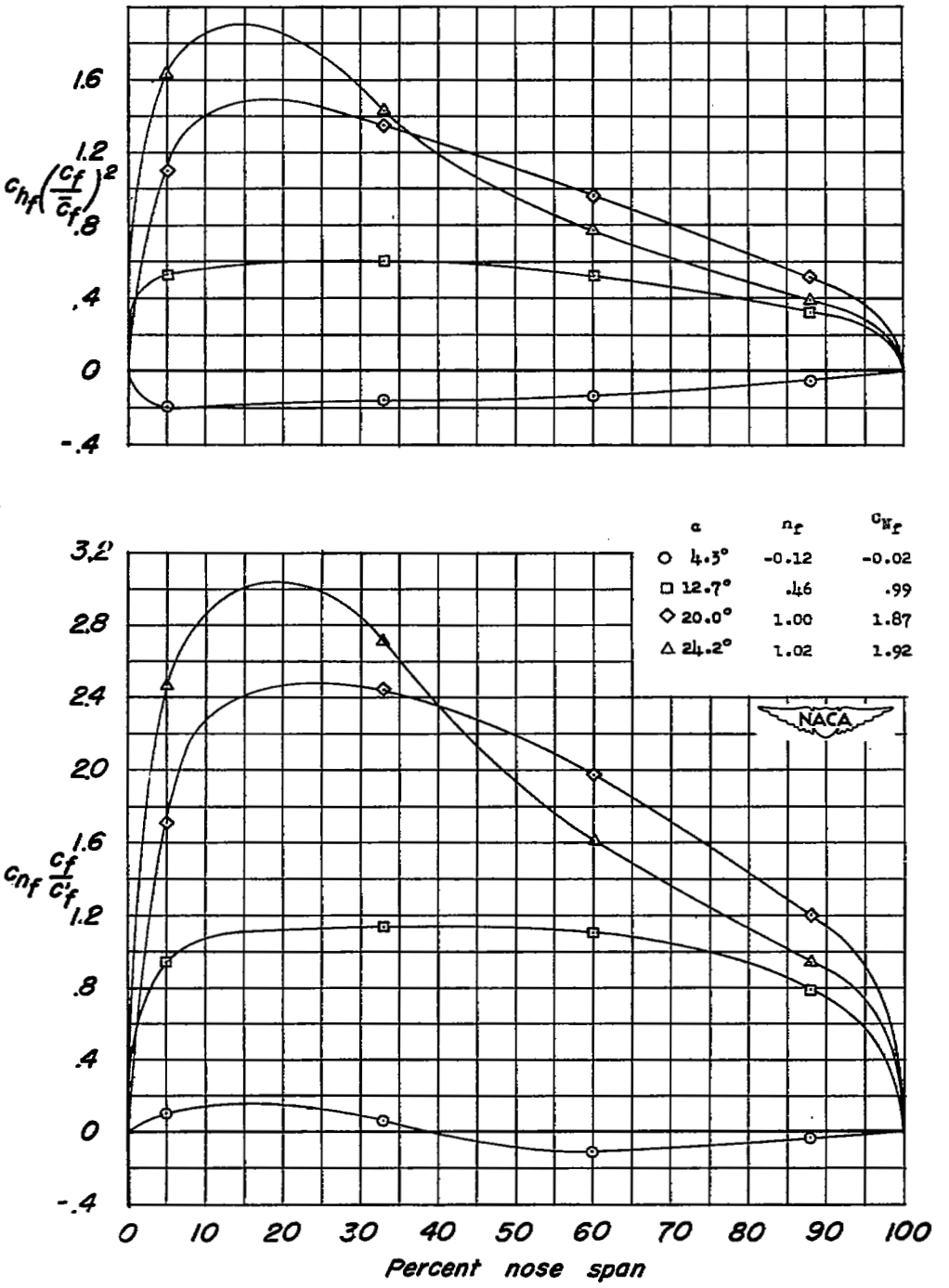

Figure 10.- Spanwise variation of drooped-nose normal-force and hinge-moment coefficients. $0.60\frac{b}{2}$-span drooped nose; $\delta_f = 30^\circ$; split flaps off.

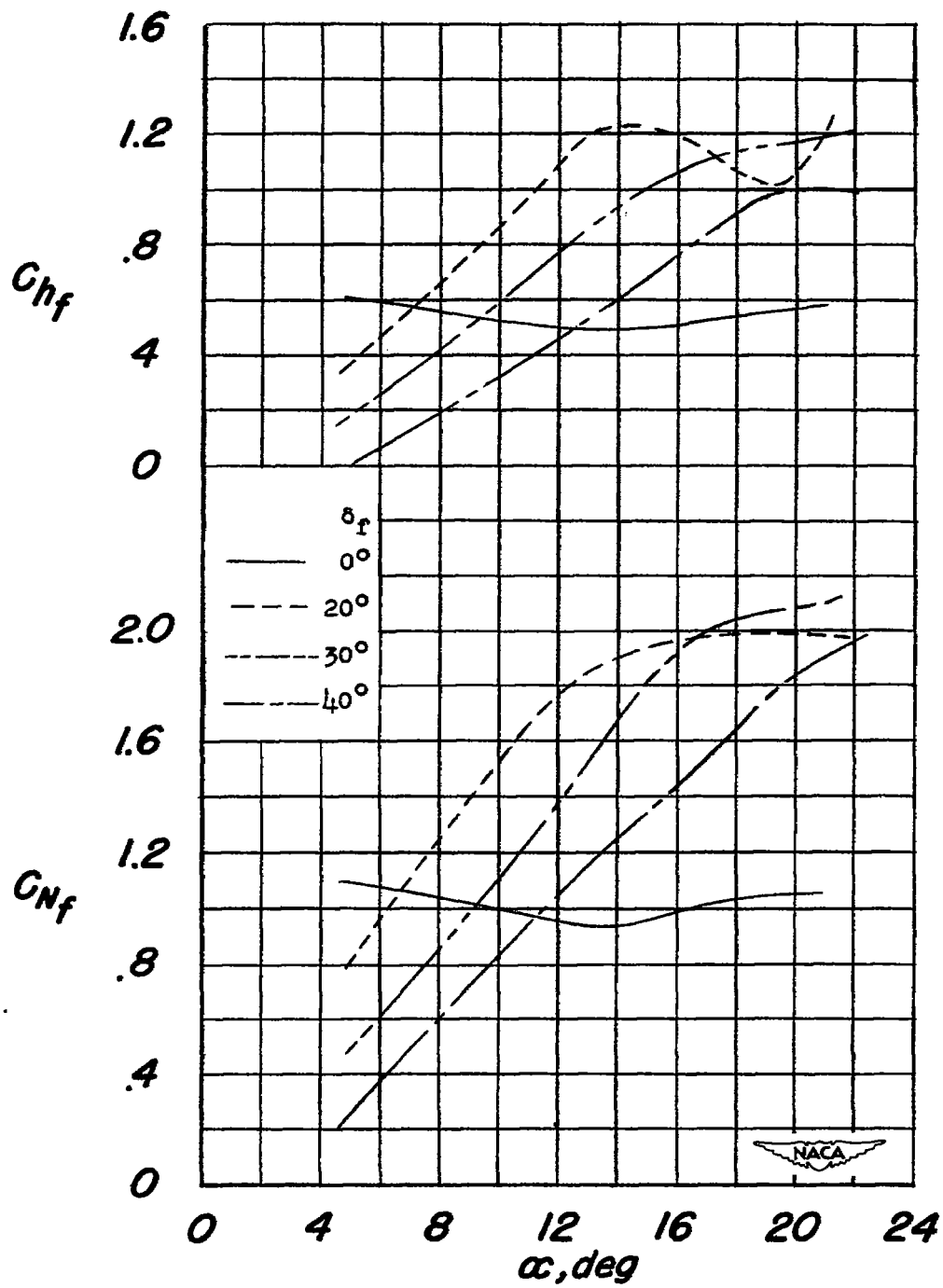

Figure 11.- Variation of drooped-nose normal-force and hinge-moment coefficients with angle of attack. $0.60\frac{b}{2}$-span drooped nose; half-span split flaps deflected 60°.

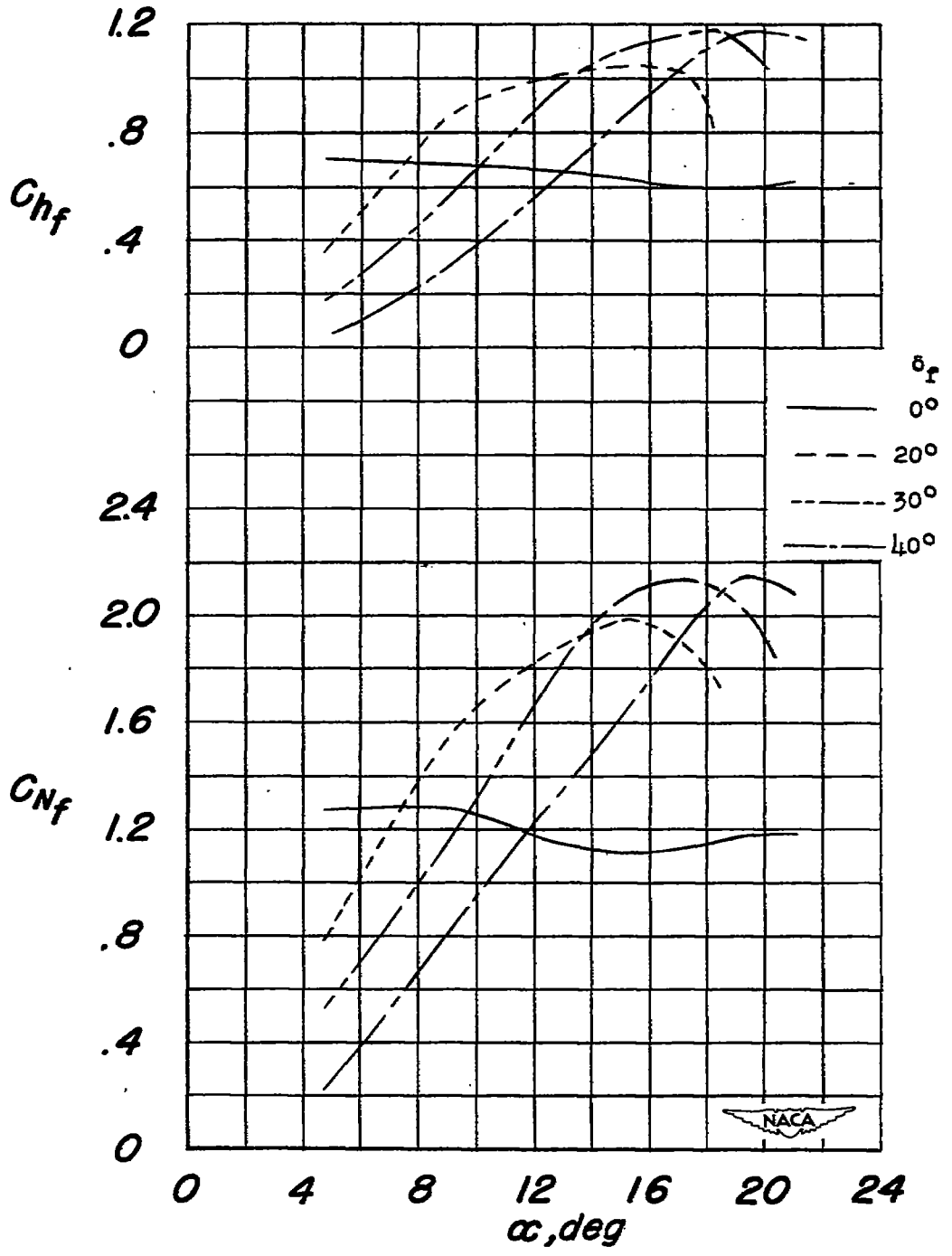

Figure 12.- Variation of drooped-nose normal-force and hinge-moment coefficients with angle of attack. $0.75\frac{b}{2}$-span drooped nose; half-span split flaps deflected 60°.

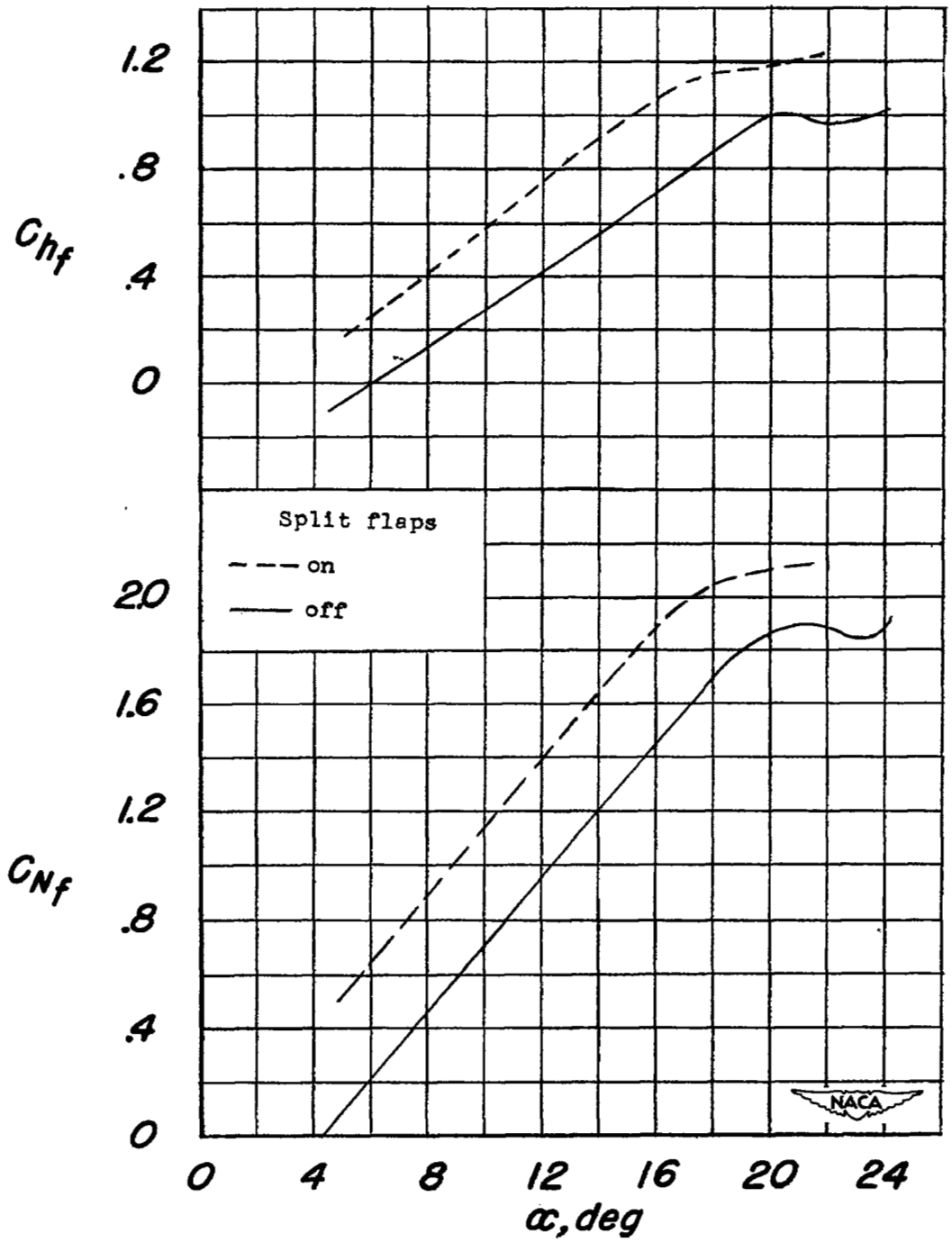

Figure 13.- Effect of half-span split flaps deflected 60° on the variation of drooped-nose normal-force and hinge-moment coefficients with angle of attack. $0.60\frac{b}{2}$-span drooped nose.